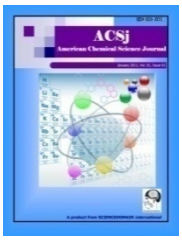

American Chemical Science Journal
3(4): 387-400, 2013

SCIENCEDOMAIN *international*
www.sciencedomain.org

Photocatalytic Activity of Titanium Oxide – Iron Oxide Coatings Prepared by Plasma Spraying

P. Ctibor[1*], V. Stengl[2] and Z. Pala[1]

[1]Institute of Plasma Physics, ASCR, Za Slovankou 3, 182 00 Praha 8, Czech Republic.
[2]Institute of Inorganic Chemistry, ASCR, 250 68 Husinec-Rez, Czech Republic.

Authors' contributions

This work was carried out in collaboration between all authors. Author PC designed the study, supervised all spray experiments, performed the analysis of reflectivity, Raman and microscopy -based tests, mechanical tests, managed the literature searches and wrote the first draft of the manuscript. Author VS, performed the powder synthesis and all photocatalytic tests. Author ZP performed all XRD-based tests. All authors read and approved the final manuscript.

Research Article

Received 4th May 2013
Accepted 18th June 2013
Published 17th July 2013

ABSTRACT

This study examines the photocatalytic activity of coatings produced by atmospheric plasma spraying (APS). The spraying tool used is a water-stabilized plasma gun WSP. The TiO_2– Fe_2O_3 powder with and without Na_2SiO_3 additive was agglomerated to build particles suitable for feeding into the plasma jet and spraying. The coatings are analyzed by scanning electron microscopy, X-ray fluorescence and X-ray diffraction. Photocatalytic degradation of acetone as well as the growth kinetics of the products - carbon dioxide and carbon monoxide - is quantified for both coating types and compared with a pure TiO_2 coating. The coatings show a lamellar structure, as is typical for this technological process. However the porosity is rather high. Anatase titania from the feedstock powder is converted to rutile phase whereas a presence of $FeTiO_3$ is detected in the coating without Na_2SiO_3. The coating from powder with Na_2SiO_3 admixture is amorphous. Both coatings are more photocatalytically active than the reference TiO_2 coating.

Keywords: TiO_2-Fe_2O_3; plasma spraying; spectroscopy; band gap; photocatalysis.

**Corresponding author: Email: ctibor@ipp.cas.cz;*

1. INTRODUCTION

When TiO_2 is illuminated by photons having energy higher than TiO_2 band gap, charge carriers are photogenerated promoting oxidation and reduction reactions. This photocatalytic activity is applied, for example, in water purification [1,2] and air cleaning [3]. The photocatalytic activity of the coatings can vary with the composition (stoichiometry, hydroxyl and impurity concentrations), porosity, and surface roughness as well as with the micro- or nano-structure [4]. Another influential factor on the photocatalytic activity is, of course, the phase composition of the material.

There exists a demand on fabrication techniques of TiO_x films (crystalline as well as amorphous) and coatings applicable to large area deposition and high quality coverings achieved even at low substrate temperatures [5].

A search for ways how to improve the photocatalytic efficiency of the TiO_2-based coatings is a desirable subject of research and development. It has been also realized that the band gap of anatase TiO_2 (about 3.2 eV) means that the electron can only be excited by the high power UV light irradiation with a wavelength shorter than 387 nm [6]. A multiple band gap photocatalytic reaction cell was formed in composite TiO_2–Fe_3O_4 coatings [7]. Part of the material reacts in plasma according the formula (1).

$$Fe_3O_4 + TiO_2 \rightarrow FeTiO_3 + Fe_2O_3 \quad (1)$$

$FeTiO_3$, as a p-type semiconductor [8] with band gap about 2.5 eV, is advantageously combined with a sub-stoichiometric TiO_2 that is n-type semiconductor, thus a solid p-n junction formation in the sprayed coating is possible [8]. The TiO_2–Fe_3O_4 coatings consisted of anatase TiO_2, rutile TiO_2 and pseudobrookite Fe_2TiO_5 phase which appeared when the content of Fe_3O_4 additive was over 10 % [6]. Relatively low addition of Fe_3O_4 led to ilmenite $FeTiO_3$ phase in the coatings. The content of anatase TiO_2 in the sprayed coatings decreased with the increasing Fe_3O_4 content. The photocatalytic activity was improved with an increase of $FeTiO_3$ content in the coating, which was explained by the good photoabsorbance and by the two-step electron transfer model [6].

During the photocatalytic reactions, when a semiconductor containing TiO_2 and $FeTiO_3$ is UV-irradiated, the electron-hole pairs possibly form in two steps [8]. In the first step the electron is initiated from the valence band to the conduction band of $FeTiO_3$, and in the second step the electron in the conduction band of $FeTiO_3$ is initiated to the conduction band of TiO_2. The benefit, called also inter-semiconductor hole-transfer mechanism [9], is to extend the light absorption range and possibly inhibit recombination of the excited holes and electrons.

The plasma sprayed TiO_2 is typically slightly sub-stoichiometric (TiO_{2-x}) [10,11]. For avoiding it in the system titanium oxide – iron oxide, we proposed the use of Fe_2O_3 instead of Fe_3O_4. In this case part of the material will follow the below-mentioned reaction (2), especially in the case of a high-temperature plasma jet of the water-stabilized plasma gun [12], utilized in our spray tests.

$$Fe_2O_3 + TiO_2 \rightarrow FeTiO_3 + FeO + O \quad (2)$$

The free oxygen, released according to the formula (2) can replace the oxygen deficiency in TiO_{2-x} resulting from the reducing environment of the plasma jet of WSP. FeO evaporates

preferentially because of its melting point at 1370ºC (boiling at 3414ºC), which is about 180ºC lower than melting points (and simultaneously decomposition points) of both Fe_2O_3 and Fe_3O_4 at 1550ºC.

Chemical synthesis of any novel powder is in the first step done without special attention to the size distribution suitable for thermal spray techniques. We describe in this paper the second step – the more targeted one. We have optimized the chemical procedure to obtain so called "feedstock for plasma spraying" with an applicable size distribution. Further we have sprayed it. The goal of the present paper is to examine the influence of plasma spray process by WSP on the composition, microstructure and photocatalytic activity of TiO_2 powder doped with Fe according to the above-described considerations.

2. EXPERIMENTAL DETAILS

2.1 Powders and Spraying

An original technique was used for preparation of the TiO_2-Fe_2O_3 composition. Ten liters of 1.6 M solution $TiOSO_4$ (99.9% purity; Sigma-Aldrich) was diluted in 60 liters of water. Than 1.6 kg of $FeSO_4$ (99.0% purity; Sigma-Aldrich) and 6 kg of urea was added. The reactive mixture was boiled at 98ºC for 8 hours, decanted, filtered and dried at 105ºC. This method is based on thermal decomposition of urea at temperature higher than 60ºC. The products of these reactions are mostly spherical agglomerates composed of sub-micrometric individual spheres.

After drying, disintegration of dry TiO_2-Fe_2O_3 large agglomerates and sieving, we obtained a feedstock for the plasma spray process with a size 63-125 μm. This feedstock is further labeled **FeT**. This powder contains TiO_2 with nominally 5 wt. % of Fe_2O_3. However, a majority of the powder disintegrated at sieving back to very fine particles, unsuitable for plasma spraying. We searched for an easy re-agglomeration process using an inorganic substance, which can be released at a thermal processing. At optimal conditions would it be a substance enhancing also structural features that promote the photo-activity. We selected Na_2SiO_3, because it can influence the surface state and phase transformations of TiO_2 [13,14]. We mixed mechanically in the ratio 1:1 the disintegrated "FeT" fine powder with so called "water glass" (containing 38 wt. % of Na_2SiO_3; the rest is silicic acid) and dried the product at room temperature for 24 hours. After careful crushing of the product and further sieving we obtained a feedstock for the plasma spray process, again with the size 63-125 μm. This feedstock is here labeled **FeT-VS**. This powder contains TiO_2 with about 4 wt. % of Fe_2O_3 and traces of Na_2SiO_3 also with possible byproducts. Considering silicic acid as "metasilicic" H_2SiO_3, it was decomposed during the drying to H_2O and SiO_2 and H_2O evaporated. By this way SiO_2 is expected in the feedstock.

The plasma gun used for spraying was a water-stabilized plasma gun (WSP) working with a d.c.-current and water vapor as a plasma-forming gas. The parameters used were: Feeding distance (FD) 105 mm; spray distance (SD) 350 mm; torch current 480 A and voltage 320 V; powder feeding gas – air (flow rate 3.25 slpm). Powder feed rate was set to 12-15 kg/h and substrates were made from carbon steel, 120x25x2.5 mm^3. The substrates were grit blasted and acetone degreased before the spraying.

The reference sample "R", sprayed using a commercial TiO_2 powder (according our XRD analysis containing about 88 wt.% - anatase; balance - rutile) prepared from a nanometric

powder by its agglomeration, was included in our experiments. The nanometric powder was Altium™ TiNano 40 VHP (Altair Nanomaterials, Reno, NV, USA). An agglomerated fraction from 45 to 75 microns in size was utilized for WSP spraying at processing conditions labeled 52-450, which means feeding distance 52 mm and spray distance 450 mm.

2.2 Characterization Techniques

X-ray diffraction (XRD) was performed on SIEMENS D500™ theta-2theta Bragg-Brentano diffractometer, using cobalt K-alpha radiation, in order to gain information about the phases present within the feedstock powder and coatings. The size of crystallites was calculated according two approaches - Williamson-Hall graph (for rutile) and Scherrer formula (for anatase peak 101). The influence of the instrumental broadening of lines was eliminated using CaF_2 standard.

Raman spectroscopy was performed using a Lambda Solutions P1 apparatus - laser wavelength 785 nm, objective magnification 50x, integration time 25 s. The surface of the coating was polished before the test.

Porosity of coatings was measured by image analysis of cross-sectional micrographs taken by a CCD camera. For analysis of light micrographs the software Lucia G (Laboratory Imaging, Czech Rep.) was used. Reported values are averages from 10 frames analyzed at 250x magnification. The surface roughness was recorded by the Surtronic 3P (Taylor Hobson, UK) using a contact technique. Microhardness was measured by a Hanemann microhardness head (Zeiss, Germany) mounted on an optical microscope with a fixed load of 1 N and a Vickers indenter. Twenty indentations from various areas of a cross section for each sample were analyzed.

Scanning electron microscopy (SEM) studies were performed using a Philips XL30 CP microscope equipped with an energy-dispersive X-ray (EDX) detector.

The reflectance measurement in this work has been implemented using a ultra-violet/visible/near-infrared (UV/Vis/NIR) spectrometer (Shimadzu, Japan). Prior to the actual measurement, the calibration process was conducted using the $BaSO_4$ reference mirror in order to minimize the error from environment. The accuracy guaranteed by the equipment manufacturer is that of wavelength ±0.3 nm and the uncertainty of the measurement less than 0.2%. The wavelength of incident light used for the reflectance measurement was in the range from 250 to 2000 nm, and the diameter of the measured area was about 2 cm^2. The corresponding band gap energy was estimated after converting the reflectance curves to absorbance and recalculation [15] to Kubelka-Munk absorbance units.

Photocatalytic decomposition of acetone was tested and the addressed coatings were compared with a reference sample “R”. Kinetics of the photocatalytic degradation of gaseous acetone was measured by using a self-constructed stainless steel photoreactor [16] with a fluorescent lamp Narva LT8WT8/073BLB, i.e. a black lamp with 365 nm wavelength and input power 8 W. Gas concentration was measured with the use of a quadrupole mass spectrometer JEOL JMS-Q100GC and a gas chromatograph Agilent 6890N. A high-resolution gas chromatography column (19091P-QO4, J & W Scientific) was used. The sample from the reactor was taken via a sampling valve at time intervals of 2 hours. The reactor with the total volume of 3.5 liters was filled with oxygen by 1 liter per minute flow rate. Whole internal space of the reactor was kept at 35ºC and the dose of acetone applied by means of a Hamilton syringe through a needle and septum. The real decomposition rates

were recalculated to a sample area 10 cm^3 before plotting into graphs. Before performing the photocatalytic test, a blank test was carried out without the photocatalyst. No significant changes in the acetone concentration were observed when the ultraviolet lamp was turned on.

Photocatalytic decomposition of gaseous NO was also tested. A flow type of reactor was used. Test conditions were: Intensity of UV light 1.5 mW/cm^2, total flow rate 1.2 L/min, initial concentration of NO – 1 ppm in nitrogen, humidity 50%, temperature 25ºC, distance between the sample and the window of photoreactor 5 mm. The test was performed following the ISO 22197-1:2007(E) standard.

3. RESULTS AND DISCUSSION

Light micrographs of the coatings FeT and FeT-VS are shown in Fig. 1. The cross section of the coating FeT shows rather porous lamellar microstructure. The coating FeT-VS is displayed in an in-plane view (spray direction) because the integrity of the coating was rather low and preparation of a well polished cross section was not possible. We can see predominantly circular pores with various sizes up to tens of micrometers.

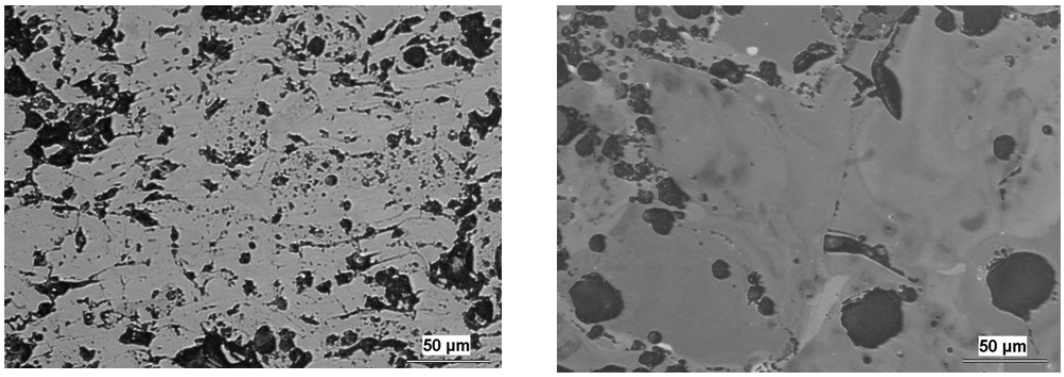

Fig. 1. FeT, light micrograph of the cross section (a) and FeT-VS, light micrograph of the in-plane section (b)

A SEM micrograph of surface of the FeT coating is displayed in the Fig. 2a. The surface contains a lot of globular particles approx. from 1 to 5 µm in diameter. These particles originate from larger agglomerated units, disintegrated in the plasma jet, which solidified probably before impact onto small globular particles adhering on the coating surface. The feedstock powder is rather irregular, Fig. 2b, with fine particles adhering on the surface only with limited compactness [17]. The coating surface, Fig. 2a, shows any pronounced flattening into lamellas and mechanical anchoring to previous layers. For such a microstructure we can preclude a low mechanical integrity of the entire coating. However the cross section, Fig. 1a, shows a partly lamellar microstructure rather typical for a plasma-sprayed coating, only with porosity higher than usually.

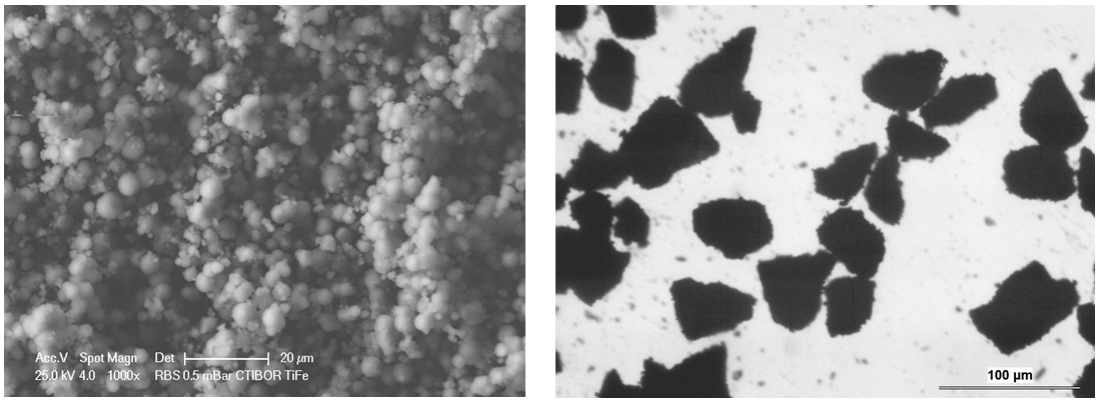

Fig. 2. Surface of the FeT plasma sprayed coating, SEM-SE (a) and FeT feedstock, light micrograph (back-light used) of the individual particles (b)

Phase composition of the FeT-VS feedstock, Fig. 3, is: anatase TiO_2, hematite Fe_2O_3 and thenardite Na_2SO_4. Sulfur in the thenardite phase originates from unreacted $TiOSO_4$ used at TiO_2 production or unreacted $FeSO_4$ from Fe_2O_3 production. The FeT coating contains rutile, anatase and ilmenite $FeTiO_3$. Semi-quantitative analysis of X-ray diffraction patterns within the crystalline material of the irradiated volume yielded the following weight percentages, 77% of rutile and 23% of anatase in the FeT-VS coating; the same analysis indicated 89% of rutile, 5% of anatase and 6% of ilmenite in the FeT coating. The FeT-VS coating contains besides rutile and anatase also amorphous material, which dominates to the XRD pattern. The average size of anatase crystallites is 10 nm for the FeT-VS feedstock, 32 nm for the FeT-VS coating and 95 nm for the FeT coating. The average size of rutile crystallites was similar for all coatings – about 150 nm.

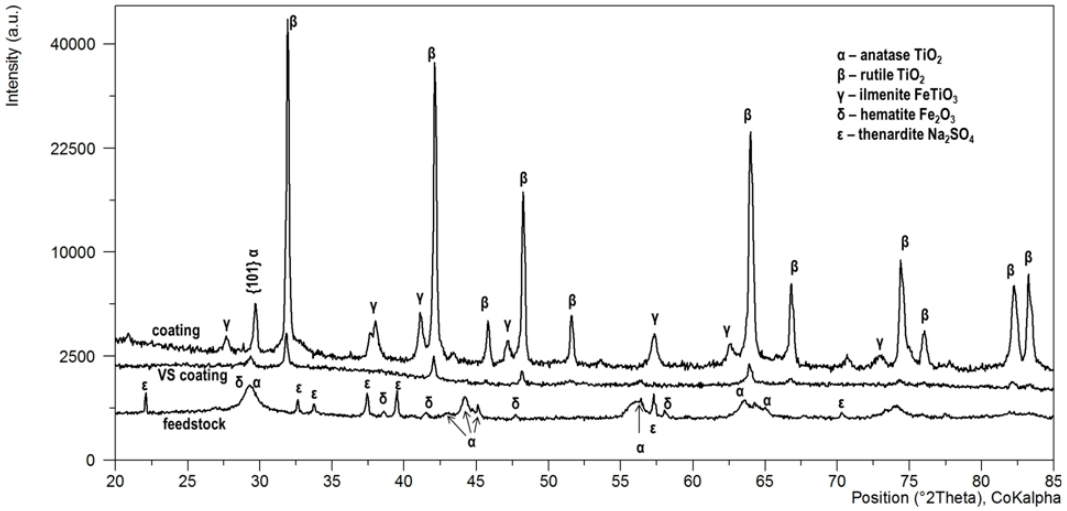

Fig. 3. XRD patterns of the FeT-VS feedstock powder, FeT (“coating”) and FeT-VS (”VS coating”)

Average porosity of the FeT coating is 28 %, whereas mean equivalent diameter of pores is 17.6 μm and maximum equivalent diameter of pores is 42.4 μm. Minimal circularity of pores is 0.041. For a comparison, a reference coating "R" exhibits porosity 8 %, whereas mean equivalent diameter of pores is 1.2 μm and maximum equivalent diameter of pores is 12.9 μm. Minimal circularity of pores is 0.061 for the R-coating,. This means that FeT coating is much more porous, pores are larger and less globular (lower circularity). FeT-VS coating with its low integrity did not allowed proper image analysis.

Table 1 shows XRF analysis of the FeT coating. The atomic ratio Ti / Fe is 4.08. Table 2 summarizes surface roughness of the coatings FeT and FeT-VS in comparison with the reference coating R. We see the high roughness of the FeT-VS coating from the viewpoint of both parameters, whereas the FeT coating has only slightly coarser surface than the reference coating R, tailored for good mechanical properties [18].

Table 1. XRF analysis of the FeT coating

Element	Wt. %	At. %
O (K)	41.79	68.94
Ti (K)	45.26	24.94
Fe (K)	12.94	6.12
Total	100.00	100.00

Microhardness of the FeT coating is 8.7 ± 1.6 GPa, whereas FeT-VS coating is less hard, 6.8 ± 1.0 GPa. The reference coating R is the hardest, 9.0 ± 1.0 GPa. As mentioned earlier, the FeT-VS coating did now allowed the cross-sectional cut; also the hardness is from the in-plane section, whereas for both other coatings the conventional cross section was used.

Table 2. Surface roughness of the coatings

Coating	R_a	$R_{y\ max}$
FeT	14.0 ± 0.5	105.2 ± 1.8
FeT-VS	23.8 ± 1.5	168.2 ± 6.7
Ref. "R"	13.3 ± 0.7	94.9 ± 9.4

Raman spectra are displayed in the Fig. 4. On the spectrogram of the FeT coating anatase peak at 399 cm^{-1} as well as rutile peak at 440 cm^{-1} are present as one wider peak centered at about 420 cm^{-1}. This feature can be also associated with an oxygen deficiency. The position of this rutile peak located at about 445 cm^{-1} shifts to low wavenumbers as the O/Ti ratio starts to decrease [19,20]. An incorporation of Fe^{3+} into TiO_2 creates large amounts of oxygen vacancies, and due to them, the E_g peak of rutile phase located around 445 cm^{-1} at zero concentration of iron ions shifts to the low wavenumbers with an increase in iron content [19]. This same feature, however much less pronounced, is presented also on the spectrum of the FeT-VS coating. Raman line shifts and broadening correspond to a thermal treatment in air and are therefore attributed to an oxygen deficiency effect [21]. In contrast, the reference coating R exhibits the rutile peak at 440 cm^{-1}. This coating, and also the FeT coating, both have the rutile peak at 610 cm^{-1}. For the FeT-VS coating this peak is not clear enough because of amorphous composition. All three coatings have the anatase peak at 144 cm^{-1}, however not very intensive.

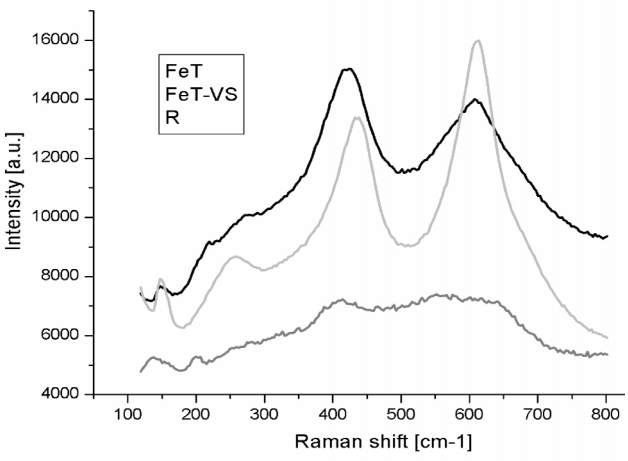

Fig. 4. Raman spectra of the coatings – FeT, FeT-VS and the reference coating R

Energy of the transfer of an electron from the valence band to the conduction band is expressed in the Fig. 5 in Kubelka-Munk absorbance units (KMU) [22]. The Kubelka–Munk intensity for the FeT coating, which is approximately 7 KMU at the experimental light wavelength of 365 nm, is lower than that of the FeT-VS coating of approximately 9 KMU but higher than the reference R coating of approximately 2 KMU. The spectra do not drop sharply in the wavelength range of 340 to 400 nm but a high K-M absorbance continues to longer wavelengths, especially for the FeT-VS coating. This is a consequence of an interaction of the metal ions (in our case Fe) with the TiO_2 catalyst [22,23]. A meaning of it is that more irradiation light energy of a broad-band source can be utilized. At the plasma spray process, also a few Fe_2O_3 powder reacted with TiO_2 powder and produced iron titanium oxide compounds, such as $FeTiO_3$, which may improve the photo-absorptive ability of the coatings in the visible spectral range [24]. Therefore, it is concluded that the photocatalytic activity of the FeT and FeT-VS coating partly results from the absorptivity of $FeTiO_3$. Na_2SiO_3 in the FeT-VS coating (without $FeTiO_3$) helps to stabilize the structural disorder most probably due to the Ti–O–Si chemical bonds [13]. Reported Fe-doped TiO_2 films [25,26] exhibited slight red-shift in absorbance and enhanced absorbance in the visible-light region compared with undoped TiO_2, attributed to bandgap narrowing by Fe^{3+} doping into TiO_2 [27], which is also supported by calculations [28]. The charge-transfer transition between dopant ions via the conduction band ($Fe^{3+} + Fe^{3+} \rightarrow Fe^{4+} + Fe^{2+}$) is mentioned as responsible for this behavior [26].

According [29] ilmenite $FeTiO_3$ is a semiconductor with band gap of about 2.6 eV approximating to that of TiO_2 (2.7 eV). Upon the irradiation of visible light, the electrons in the valence band (VB) of $FeTiO_3$ are excited to CB. Thus, the VB of $FeTiO_3$ becomes partly vacant; consequently electrons in VB of TiO_2 can be transferred to that of $FeTiO_3$ due to their similarity in energy level, leaving behind the holes in VB of TiO_2. On the other hand, when the material is irradiated by UV–Vis light, electrons in VB of TiO_2 are excited to CB which can be transferred to CB of $FeTiO_3$ because the flat-band potential of TiO_2 is 0.53 V higher than that of $FeTiO_3$. Consequently, electron–hole pairs are well separated and electrons in ilmenite surface have sufficient lifetime for the raction with a polutant.

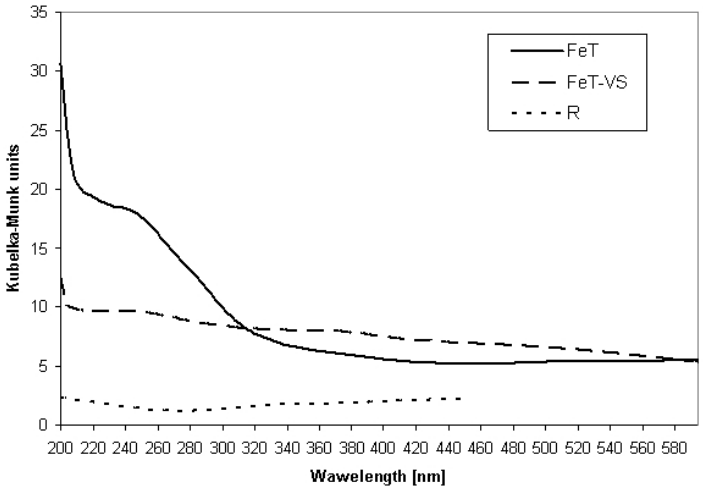

Fig. 5. Energetic comparison of the transfer of an electron from the valence band to the conduction band for all coatings – FeT, FeT-VS and the reference coating R (measured only until 450 nm)

Therefore, the photoactivity improvement along with increasing content of $FeTiO_3$ in the mixed $FeTiO_3$-TiO_2 system is reasonable.

Concerning the photocatalytic degradation of acetone, its concentration as well as carbon dioxide and carbon monoxide concentrations were detected at retention times up to 40 hours, see Fig. 6. Among the three studied coatings the less photoactive one is the reference coating R. The initial concentration of acetone decreased in this case from 1 to 0.93 after 40 hours, Fig. 6a. The acetone concentration decreased from 1 to 0.87 after 40 h and from 1 to 0.84 after 40 h for FeT and FeT-VS coating, respectively. For R coating and for FeT coating the course of the kinetic curve is linear whereas for FeT-VS coating is the drop between linear and logarithmic trend. This partial slowing of the reaction could be related to saturation effect. For acetone a direct process without any semi-product is the relevant scenario [30].

A carbon dioxide concentration growth, Fig. 6b, was very similar for FeT-VS and R coatings, whereas the FeT coating produced even higher quantity of CO_2. For R coating the growth is linear. For FeT and FeT-VS coating the course follows the power law with exponents 0.537 and 0.525, respectively.

A carbon monoxide concentration growth, Fig. 6c, was the highest for the FeT-VS coating and lower for the R coating, whereas the FeT coating has lower quantity of produced CO. The course follows the power law for R and FeT-VS coatings (with exponents 0.465 and 0.482, respectively) whereas for the FeT coating is the growth logarithmic. The tendency to saturation is much more pronounced for this coating. From the comparison with CO_2 kinetics is visible that the FeT coating converts more acetone to CO_2 than to CO when compared with the two other coatings.

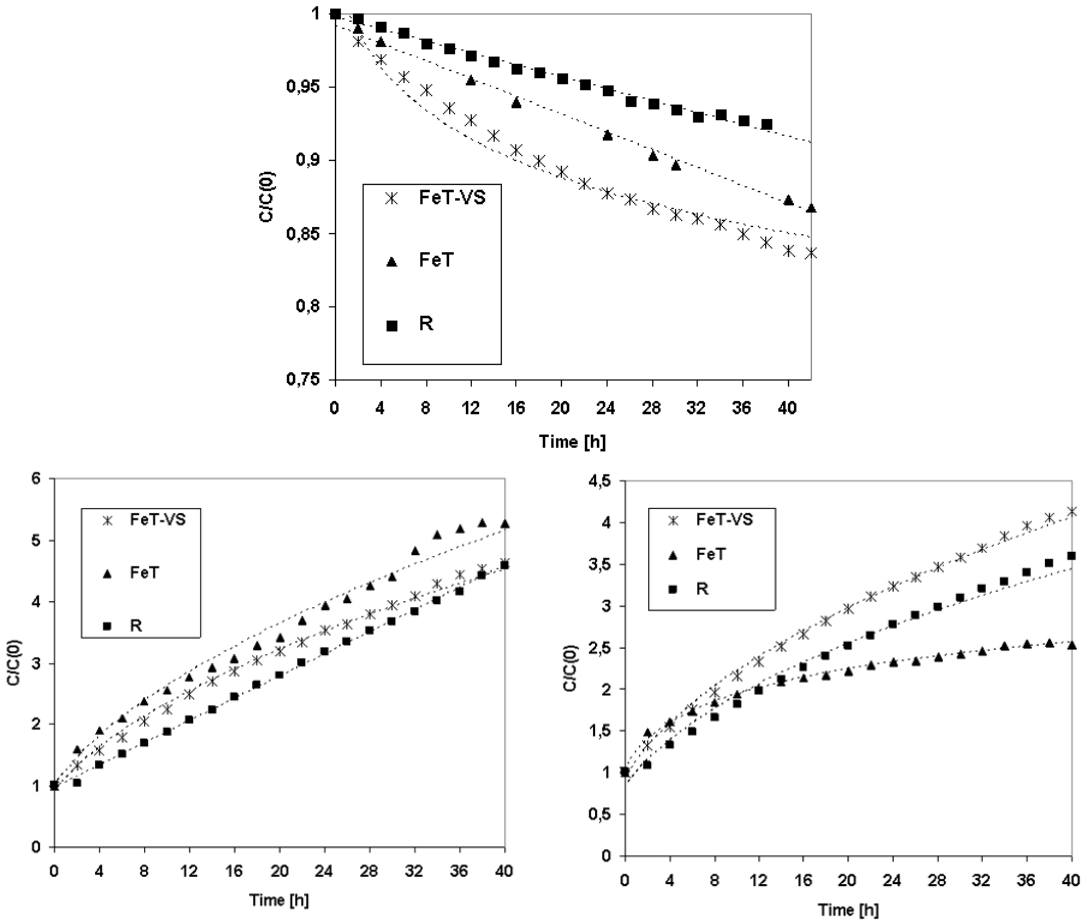

Fig. 6. Photocatalytic decomposition of acetone and concentration growth (a) of the reaction products – carbon dioxide (b) and carbon monoxide (c)

The FeT-VS coating is predominantly amorphous but its photoactivity, in terms of acetone decomposition speed, is even higher. In [31, 32] was shown that variously fabricated coatings with a limited crystallinity were better photocatalysts than other, more crystalline samples. Typically is it mentioned also together with the influence of OH groups, also detected in the past on a surface of our TiO_2-based plasma sprayed coatings [33]. Also FeT and FeT-VS coatings provide better photoactivity than the TiO_2 reference coating R because of mechanisms mentioned in the case of Ti-doped α-Fe_2O_3-based films [34]. The anatase crystallite size is smaller for the FeT-VS coating compare to FeT coating and the anatase quantity higher in FeT-VS. According to the literature the small crystallite size can enhance the photoactivity of the TiO_2-based coatings [31].

Concerning the interpretation the role of sulphur is it eligible to point out the following factors. Sulphur species were coordinated with TiO_2 in the network producing more acidic sites on the TiO_2 surface [34]. These acidic sites could capture more photo-induced electrons that could effectively protect the photo-induced holes from recombination with electrons. Thus,

the quantum efficiency of the TiO_2 photocatalyst is improved by sulphur doping, resulting in the higher photocatalytic activity (tested on methyl orange solution in [34]).

Fe-N-S-tridoped TiO_2 photocatalysts were synthesized by one step in the presence of ammonium ferrous sulfate [35]. Fe (III) and S^{6+} were incorporated into the lattice of TiO_2 through substituting titanium atoms, and N might coexist in the forms of substitutional N (O-Ti-N) and interstitial N (Ti-O-N) in tridoped TiO_2. Fe-N-S-tridoped TiO_2 catalyst exhibited a higher visible light photocatalytic activity for the degradation of phenol than that of pure TiO_2 and Degussa P25 TiO_2 [35].

The photocatalytic test duration for degradation of NO was only 70 min. The relative photonic efficiency was constantly about 3 % for both Fe-containing coatings and also for the reference coating R. The process involved is photo-oxidation of the NO onto HNO_2, which is immediately converted to NO_2 and in some cases also on HNO_3. The quantity of the products was not monitored.

The photoactivity of all coatings appears much higher for the acetone than for the nitric oxide. Such a difference is difficult to explain, but some of the rarely published results of tests utilizing more than one chemical substance (on more than one test setup) for a comparison of photocatalysts show similar discrepancies [36-38]. For example the activity of powdered mesoporous photocatalysts correlates with their surface area and pore volume for gas phase reaction, whereas in the case of a liquid phase organophosphorous compound (dimethyl methylphosphonate) oxidation, there is no sufficient correlation [36]. In another work [37] the photocatalytic conversion of toluene by the TiO_2-modified concrete surface layer was not detected, although nitric oxide could be effectively removed in the same operation. Our titanium oxide – iron oxide coatings exhibit selectivity for gaseous acetone whereas gaseous nitric oxide is decomposed is decomposed in different test only with low efficiency.

4. CONCLUSIONS

The goal of this study was to examine the photocatalytic activity of coatings produced by atmospheric plasma spraying (APS). The plasma spray system used was a water-stabilized plasma gun (WSP) whereas TiO_2–Fe_2O_3 powder with and without Na_2SiO_3 additive was agglomerated into particles suitable for plasma feeding and spraying.

Anatase titania from the feedstock powder was mainly converted to rutile phase whereas also $FeTiO_3$ was detected in the coating without Na_2SiO_3. The coating from powder with Na_2SiO_3 was predominantly amorphous. The addressed WSP coatings were more photocatalytically active than a reference TiO_2 coating without Fe. At the spray procedure, some Fe_2O_3 powder reacted with TiO_2 powder and produced $FeTiO_3$. The coating with Na_2SiO_3 admixture has even finer anatase crystallites and a large amorphous portion. Its UV-photoactivity was even higher for acetone, whereas gaseous nitric oxide was decomposed on all studied coatings only with relatively low efficiency.

ACKNOWLEDGMENTS

This work was supported by the Grant Agency of the Academy of Sciences of the Czech Republic (Project No. IAAX00430803). The authors thank to V. Kalousek (J. Heyrovsky Institute of Physical Chemistry AS CR) for the photocatalytic test with nitric oxide.

COMPETING INTERESTS

Authors have declared that no competing interests exist.

REFERENCES

1. Molinari R, Pirillo F, Falco M, Loddo V, Palmisano L. Photocatalytic degradation of dyes by using a membrane reactor, Chem. Eng. Process. 2004;43:1103-1114.
2. Serpone N, Texier I, Emeline AV, Pichat P, Hidaka H, Zhao J. Post-irradiation effect and reductive dechlorination of chlorophenols at oxygen-free TiO2/water interfaces in the presence of prominent hole scavengers. J. Photochem. Photobiol. A-Chem. 2000;136:145-155.
3. Canela MC, Alberici RM, Sofia RCR, Eberlin MN, Jardim WF. Destruction of malodorous compounds using heterogeneous photocatalysis, Environ. Sci. Technol. 1999;33:2788-2792.
4. Boukrouh S, Bensaha R, Bourgeois S, Finot E. Marco de Lucas M.C., Reactive direct current magnetron sputtered TiO_2 thin films with amorphous to crystalline structures. Thin Solid Films. 2008;516:6353–6358.
5. Ju Y, Li L, Wu Z, Jiang Y, Effect of Oxygen Partial Pressure on the Optical Property of Amorphous Titanium Oxide Thin Films. Energy Procedia. 2011;12:450–455.
6. Ye FX, Tsumura T, Nakata K, Ohmori A. Dependence of photocatalytic activity on the compositions and photo-absorption of functional TiO_2–Fe_3O_4 coatings deposited by plasma spray. Materials Science and Engineering B. 2008;148:154–161.
7. Ye FX, Ohmori A. The photocatalytic activity and photo-absorption of plasma sprayed TiO_2–Fe_3O_4 binary oxide coatings. Surf. Coat. Technol. 2002;160:62–67.
8. Ye FX, Ohmori A, Li Ch. New approach to enhance the photocatalytic activity of plasma sprayed TiO_2 coatings using p-n junctions. Surf. Coat. Technol. 2004;184:233–238.
9. Kim YJ, Gao B, Han SY, Jung MH, Chakraborty AK, Ko T, Lee Ch, Lee WI. Heterojunction of $FeTiO_3$ nanodisc and TiO_2 nanoparticle for a novel visible light photocatalyst. J. Phys. Chem. C. 2009;113(44):19179-19184.
10. Lima RS. B.R. Marple: From APS to HVOF spraying of conventional and nanostructured titania feedstock powders: a study on the enhancement of the mechanical properties, Surf. Coat. Technol. 2006;200:3428– 3437.
11. Bozorgtabar M, Rahimipour M, Salehi M, Jafarpour M. Structure and photocatalytic activity of TiO_2 coatings deposited by atmospheric plasma spraying. Surf. Coat. Technol. 2011;205:229–231.
12. Ctibor P, Hrabovsky M. Plasma sprayed TiO_2: The influence of power of an electric supply on particle parameters in the flight and character of sprayed coating. J. Europ. Ceram. Soc. 2010;30:3131–3136.
13. Zheng H, Wang Ch, Zhang A, Zhang L, Xia S, Zhao Z. Effect of Na_2SiO_3 on synthesis of TiO_2 nanopowders by thermal processing of the precursor. Advanced Powder Technology. 2011;22:581–586.
14. Rahman MA, Kaneco S, Suzuki T, Katsumata H, Ohta K, Shafiqul Alam AM. Development of sintering materials by sea sediments and TiO_2 for the cleaning technology. Pak. J. Anal, Environ, Chem. 2007;8(1 & 2):26–35.
15. Christy AA, Kvalheim OM, Velapoldi RA. Quantitative analysis in diffuse reflectance spectrometry: A modified Kubelka-Munk equation, Vibrational Spectroscopy. 1995;9:19-27.

16. Ctibor P, Ageorges H, Stengl V, Murafa N, Pis I, Zahoranova T, Nehasil V, Pala Z. Structure and properties of plasma sprayed $BaTiO_3$ coatings: Spray parameters versus structure and photocatalytic activity. Ceram. Intl. 2011;37:2561–2567.
17. Kumar S, Selvarajan V, Padmanabhan PVA, Sreekumar KP. Spheroidization of metal and ceramic powders in thermal plasma jet: Comparison between experimental results and theoretical estimation. J. of Mater Process. Technol. 2006;176:87–94.
18. Ctibor P, Neufuss K, Chraska P. Microstructure and abrasion resistance of plasma sprayed titania coatings. J. Thermal Spray Technology. 2006;15(4):689-694.
19. Wang XH, Li J-G, Kamiyama H, Ishigaki T. Fe-doped TiO_2 nanopowders by oxidative pyrolysis of organometallic precursors in induction thermal plasma: synthesis and structural characterization. Thin Solid Films. 2006;(506–507):278–282.
20. Martyanov IN, Berger T, Diwald O, Rodrigues S, Klabunde KJ. Enhancement of TiO_2 visible light photoactivity through accumulation of defects during reduction–oxidation treatment. J. Photochem. and Photobiol. A: Chemistry. 2010;212:135–141.
21. Robert TD, Laude LD, Geskin VM, Lazzaroni R, Gouttebaron R. Micro-Raman spectroscopy study of surface transformations induced by excimer laser irradiation of TiO_2. Thin Solid Films. 2003;440:268–277.
22. Anpo M. Use of visible light. Second-generation titanium oxide photocatalysts prepared by the application of an advanced metal ion-implantation method. Pure Appl. Chem. 2000l;72(9):1787–1792.
23. Huang J-M, Li Y-X, Zhao G-D, Cai X-P. Photocatalytic degradation characteristic of amorphous TiO_2-W thin films deposited by magnetron sputtering. Trans. Nonferrous Met. Soc. of China. 2006;16:280-284.
24. Smirnova N, Eremenko A, Rusina O, Hopp W, Spanhel L. Synthesis and characterization of photocatalytic porous Fe^{3+}/TiO_2 layers on glass. J. Sol-Gel Sci. Technol. 2001;22:109-113.
25. Li Z, Shen W, He W, Zu X. Effect of Fe-doped TiO_2 nanoparticle derived from modified hydrothermal process on the photocatalytic degradation performance on methylene blue. J. Hazardous Mater. 2008;155:590–594.
26. Navio JA, Colon G, Litter MI, Bianco GN. Synthesis, characterization and photocatalytic properties of iron-doped titania semiconductors prepared from TiO_2 and iron (III) acetylacetonate. J. Molecular Catalysis A: Chemical. 1996;106:267-276.
27. Ghorai TK, Chakraborty M, Pramanik P. Photocatalytic performance of nano-photocatalyst from TiO_2 and Fe_2O_3 by mechanochemical synthesis. J. Alloys and Compounds. 2011;509:8158– 8164.
28. Wellia DV, Xu QC, Sk MA, Lim KH, Lim TM, Yang Tan TT. Experimental and theoretical studies of Fe-doped TiO_2 films prepared by peroxo sol-gel method. Applied Catalysis A: General. 2011;401:98–105.
29. Truong QD, Liu J-Y, Chung C-C, Ling Y-C. Photocatalytic reduction of CO_2 on $FeTiO_3/TiO_2$ photocatalyst. Catalysis Communications. 2012;19:85–89.
30. Mattsson A, Oesterlund L. Adsorption and Photoinduced Decomposition of Acetone and Acetic Acid on Anatase, Brookite, and Rutile TiO_2 Nanoparticles. J. Phys. Chem. C. 2010;114:14121–14132.
31. Wang G, Ling Y, Wheeler DA, George KEN, Horsley K, Heske C, Zhang JZ, Li Y. Facile synthesis of highly photoactive α-Fe_2O_3-based films for water oxidation. Nano Letters. 2011;11:3503–3509.
32. Lee Ch, Choi H, Lee Ch, Kim H. Photocatalytic properties of nano-structured TiO_2 plasma sprayed coating, Surf. Coat. Technol. 2003;173:192–200.

33. Ctibor P, Pala Z, Sedlacek J, Stengl V, Pıs I, Zahoranova T, Nehasil V. Titanium dioxide coatings sprayed by a water-stabilized plasma gun (WSP) with argon and nitrogen as the powder feeding gas: differences in structural, mechanical and photocatalytic behavior. Journal of Thermal Spray Technology. 2012;21(3-4):425-434.
34. Liu Y, Liu J, Lin Y, Zhang Y, Wei Y. Simple fabrication and photocatalytic activity of S-doped TiO_2 under low power LED visible light irradiation, Ceram. Intl. 2009;35:3061–306.
35. Li B, Cheng X, Yu X, Yan L, Xing Z. Synthesis and Characterization of Fe-N-S-tri-Doped TiO_2 Photocatalyst and Its Enhanced Visible Light Photocatalytic Activity, Advances in Materials Science and Engineering; 2012. Article ID 348927, 5 pages.
36. Kozlova EA, Vorontsov AV. Influence of mesoporous and platinum-modified titanium dioxide preparation methods on photocatalytic activity in liquid and gas phase, Applied Catalysis B: Environmental. 2007;77:35–45.
37. Chen J, Kou S-C, Poon C-S. Photocatalytic cement-based materials: Comparison of nitrogen oxides and toluene removal potentials and evaluation of self-cleaning performance. Building and Environment. 2011;46:1827-1833.
38. Ahmed S, Rasul MG, Brown R, Hashib MA. Influence of parameters on the heterogeneous photocatalytic degradation of pesticides and phenolic contaminants in wastewater: A short review. J. Environmental Management. 2011;92:311-330.

Peer-review history:
The peer review history for this paper can be accessed here:
http://www.sciencedomain.org/review-history.php?iid=242&id=16&aid=1673